*Rev. Roum. Sci. Techn.– Électrotechn. et Énerg.*
Vol. **68**, *1*, pp. 12–17, Bucarest, 2023

# INFLUENCE OF THE SAMPLING FREQUENCY ON VARIOUS MAXIMUM POWER POINT TRACKING COMMANDS

WASSILA ISSAADI [1], SALIM ISSAADI [2]

**Keywords: Intelligent neural networks; Frequency sample rate; Smoothness of the power signal; Low ripple rate; Photovoltaic maximum power point tracking (MPPT); Photovoltaic (PV) system.**

**The present work continues *the previous* article published in the International Journal of Energy (Elsevier, 2019). Our previous study aimed to develop a new, innovative method based on neural network algorithms to predict an instantaneous command. A new control strategy for photovoltaic systems was presented in [1]. This command is based on the neuronal network (NN) technique. To our knowledge, this technique has never been used in this field for that objective. The authors of this work used it to synthesize control laws for electronic power converters.**

**It should be noted that the newly designed algorithm based on neural networks is expected to be more robust with a good performance concerning tracking speed and precision. Moreover, the present research work aims at providing a robust neural structure against noisy empirical data, thus allowing the prediction of a new command. Indeed, in the current work, we will examine the parameters affecting four MPPT controls in addition to the new neural network-based algorithm developed in [1].**

## 1. INTRODUCTION

Photovoltaic solar energy directly converts a portion of solar radiation into electrical energy. This energy conversion is carried out using a photovoltaic (PV) cell based on a physical phenomenon known as the photovoltaic effect of producing an electromotive force when the cell's surface is exposed to light. The generated voltage can vary depending on the materials used to manufacture the cell. The combination of several ones PV seriated/parallel results in a generator (GPV) that is a characteristic non-linear current-voltage with a maximum power point [1–3].

The characteristic I-V of the GPV depends on the lighting level and temperature of the cell and all aging. Moreover, the operating point of the GPV is directly dependent on the load it supplies. Therefore, a matching stage between GPV and the load to couple the two elements as perfectly as possible is presented to extract every moment the maximum power available with terminal GPV [1–4].

The perfect matching problem between a photovoltaic generator and a continuous load must be solved. A technological obstacle in this type of coupling is the problem of the transfer of maximum power from the photovoltaic generator (GPV) to the load, which often needs better adaptation. The operating point is sometimes far from the maximum (MPP) power. The literature provides many solutions on the control algorithm that searches for maximum power point when the GPV is coupled to a load through a static converter [5–15].

Static converters suitable for solar PV are often called “solar dc/dc converters” in the trade. They aim to adapt the electrical energy from photovoltaic panels to power alternative-fueled loads.

Some regulators seek the optimum point of operation named MPP (maximum power point) corresponding to a voltage and an optimal PV panel current (appointed, respectively $I_{op}$ and $V_{op}$) for that the tracking of the maximum power depends on several physical parameters [7,8].

Indeed, optimizing energy in a photovoltaic conversion chain is still a subject of study. Tracking the maximum power point is considered the most relevant solution to ensure the maximum power extraction that a photovoltaic generator can provide key elements of any PV system. Several methods of maximum power point tracking (MPPT) have been developed and presented. Many of them have proven themselves experimentally. The literature offers many solutions for the MPPT control algorithm.

This article proposes a new MPPT command based on artificial neural networks (ANN). It is the first time this article's authors have suggested this command. To present this command, a quick analysis of the operation of three classic MPPT commands is given to understand the properties of the maximum power point generated by each. A study was made possible thanks to a rich experimental database describing the operation of these three different MPPT commands and the resulting ripple rate around their MPPs.

Artificial Neural Networks (NN) offer several possibilities and solutions to problems related to modelling, identification, and control.

Indeed, this work has developed a new configuration different from those already proposed for the old neural MPPT algorithms. We will test the robustness of all four MPPT commands against different acquisition system sampling frequencies. Finally, we use the better MPPT control with a better ripple rate and less loss.

The tracking results of the Neuronal algorithm and the power yields are very satisfactory compared with those of the classical MPPT algorithms developed in this study.

The sampling frequency is another parameter influencing the work of a **dc/dc converter**. Indeed, the sampling frequency is an essential parameter of tracking an MPP, particularly when determining photovoltaic system response time, the ripple, and mainly loss of power.

In addition, this work is an analysis and comparative study between four MPPT techniques, including the new technical algorithm based on neural networks developed in [1] in all aspects begotten by changing the sampling frequency.

A deduction on the best MPPT command that reaches the maximum power point with the most excellent execution speed is made, and that which generates the MPP with a

[1,2] Electrical Engineering Laboratory, Faculty of Technology, University of Bejaia, 06000 Bejaia, Algeria,
[1,] Université Mouloud Mammeri de Tizi-Ouzou, Faculté de Génie Electrique et Informatique (FGEI), Département d’Automatique, E-mail: milissa_eln@rocketmail.com
[2]3661 Boulevard Mountainview, Saint-Hubert, J3Y5N7, Québec, Canada, E-mail: Salim.issaadi@yahoo.ca

low ripple rate is detected.

## 2. DIFFERENT ALGORITHMS OF COMMANDS

### 2.1. ALGORITHM PERTURBATION AND OBSERVATION (P&O)

The P&O algorithm is called “hill-climbing”. Both names refer to the same algorithm depending on how it is implemented. Hill-climbing consists of a perturbation on the duty cycle of the power converter and P&O, a perturbation in the operating voltage of the dc link between the PV array and the power converter. In the case of hill-climbing, perturbing the duty cycle of the power converter implies modifying the voltage of the dc link between the PV array and the power converter, so both names refer to the same technique [21–30].

### 2.2. IMPROVEMENT OF PERTURBATION AND OBSERVATION (P&O) ALGORITHM

To overcome the significant disadvantage of the deviation of the P&O method when searching the MPP, HANNES proposes an improved version of this algorithm during the rapid rise of insolation levels [31–36]. The latter introduced a new condition in the “Yes” branch of the condition in $\Delta P_{pv}(k) > 0$, the flowchart structure of the P&O algorithm [1–3].

If the sign $\Delta P_{pv}(k)$ is positive during the last two previous cycles or if the direction of the disturbance was in the same direction in the last two cycles, then the direction of the next disturbance will be reversed concerning the previous direction without the need to hold taking power into account.

All the possible combinations are counted in 16 possible combinations having as inputs $\Delta P_{pv}(k)$, $\Delta P_{pv}(k\text{-}1)$, $\Delta V_{ref}(k)$, $\Delta V_{ref}(k\text{-}1)$, and as resulting output for the direction of the next disturbance, the reference voltage $\Delta V_{ref}(k+1)$.

Therefore, this improvement is quite the opposite of the simple P&O method, where the increase in the output power twice successively in the same direction of the disturbance can result from a deviation from the true MPP. While in the improved version, if the increase in output power is caused by the disturbance of the output voltage and not by an increase in the insolation, the value for $P(k)$ will decrease immediately in the opposite direction proposed by the control and thus the return to the previous direction.

If an increase in insolation causes an increase in power, the power will still increase even with this reversal of the disturbance. Therefore, the system will oscillate around its previous operating point until the increase in insolation ends.

### 2.3. INCREMENTAL CONDUCTANCE

The incremental conductance algorithm is because the slope of the curve power vs. voltage (current) of the PV module is zero at the MPP, positive (negative) on the left of it and negative (positive) on the right VP = 0 (IP = 0) at the MPP [1–5,9,35].

### 2.4. CONCEPTS OF NEURONAL COMMANDS

#### 2.4.1. ORDERING PROCESS BY BACKPROPAGATION

We will try in what follows to develop a neural controller, free of any burden imposed by the PV system, which requires putting into play climate variables. And this is to improve quality control in all its perspectives, probably enhancing power efficiency [1,37].

Accordingly, the reasoning above, we structured the block diagram in Fig. 1, the overall operation of the system in the presence of the neural controller. Note that in the case of a resistive load, the feedback information on the voltage across the load (battery) is unnecessary for the neural controller.

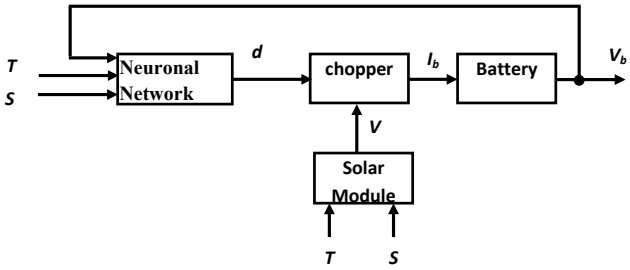


Fig. 1 – Structure of the control system by the neural network [1].

We chose a four-layer structure: an input layer, an output layer, and two hidden layers with 10 neurons, respectively, in the first and eight in the second. Another problem must be overcome by determination, not learning, done by trial and error.

## 3. OPERATION IN STABLE ENVIRONMENTAL CONDITIONS

For this series of simulations, the temperature parameter T and sunshine S are constantly maintained equal to standard test conditions, respectively $T$ = 25 °C and $S$ = 1000 W/m². The main interest will be focused on the power ripple caused by oscillations around the PPM, and its dependence on the sampling frequency of various technical MPPT and the dc-dc chopper used [1–6].

### 3.1. THE METHOD OF P&O

Figure 2 shows the panel output signal, the controller's duty ratio (d), and the operating voltage. The system is combined with a buck chopper [11–18].

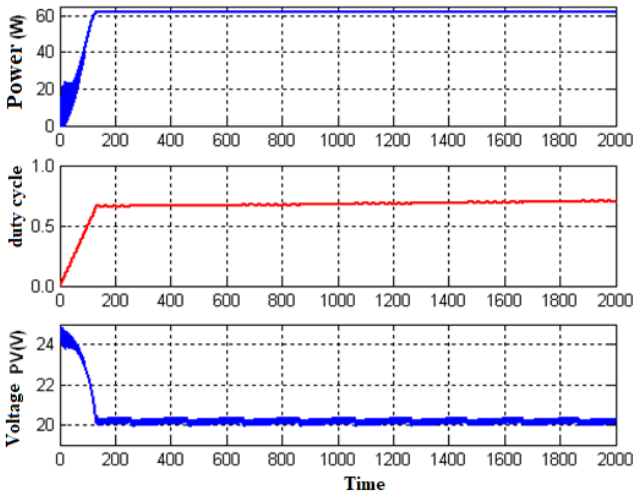


Fig. 2 – MPPT simulation of the P&O method combined with a buck chopper under stable environmental conditions ($T$ = 25 °C and $S$ = 1000 W/m²).

We note that the controller still adjusts the duty cycle $d$ quickly to reach a stable power level.

The simulation in Fig. 3 shows the actual case of the controller that can never achieve the optimal cycle report $d$ but continues to oscillate around a limit value [1–3].

The amplitude of the control oscillation depends directly on the sample rate (as we shall see in Fig. 4), and the

constant increment given to the controller. The latter, when it is essential, enables rapid convergence to the appropriate controller PPM with an accuracy near, which gives rise to oscillations of the command around a specific value, which in turn generates oscillations of power in Fig. 3, which implies losses which are proportional to the value of the constant increment and vice versa [1–3].

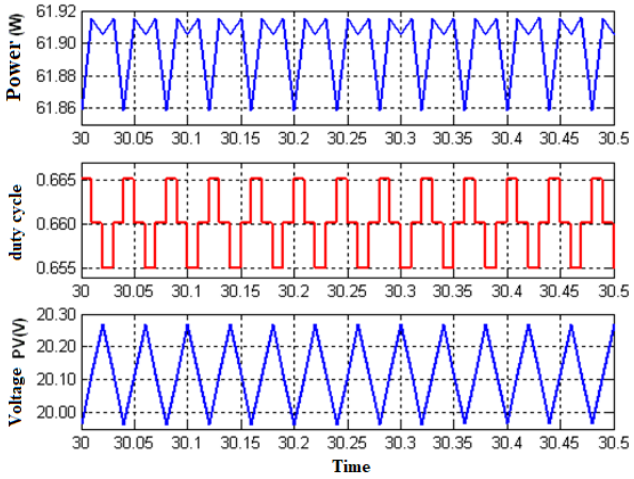


Fig. 3– Detailed graph of the power signals, duty cycle, and the output voltage of the PV module generated by the P&O MPPT method, combined with a buck chopper, for a sampling frequency of 100 Hz.

But for abrupt and rapid changes in operating conditions, it is necessary to increase the sampling frequency of the system so that the controller can appropriately bring the control output to the PPM as quickly as possible. Figure 4 shows the effect of the high sampling rate on the different output signals, which appear from a specific value as a permanent wave. This is due to the dc-dc converter, which can no longer track rapid variations of the cyclic ratio. Output power continues to fall or grow despite reversing the direction of the disturbance. In this case, the tracking mechanism is disturbed by the false information about the direction of variation of the power caused by the response delay of the dc-dc converter. This defect considerably increases the output power ripple factor, which also depends on the type of dc-dc converter used [1].

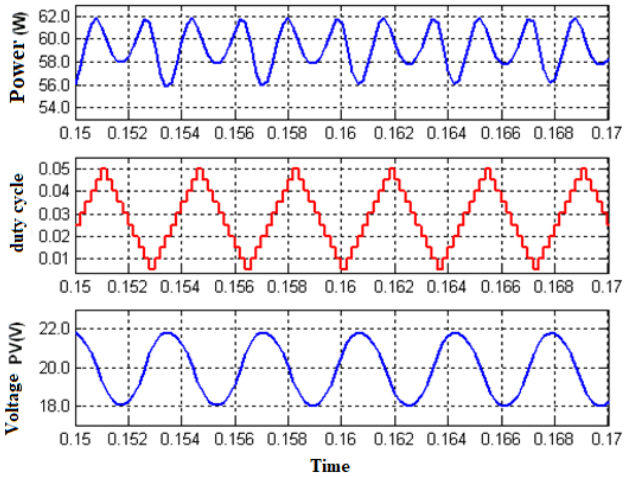


Fig. 4 – Oscillation of the P&O MPPT in high sampling frequency method combined with a buck chopper at a sampling frequency of 1 kHz.

Figure 4 shows this phenomenon for a sampling frequency of 1 kHz. It is seen that the increment is multiplied by a particular value, which multiplies the ripple rate of the power or the output voltage by the same factor [1].

This rate also depends on the capacitive components of the dc-dc converter and the converter type (buck, boost, and buck-boost). The value of the ripple factor is proportional to the input capacitors C1 and C2 output. To lower this rate, it is advantageous to reduce the capacity of the capacitors, which makes it necessary to increase the switching frequency of the PWM [1].

Other simulations are shown in Fig. 5 for a solar power supply system with the P&O MPPT method using a Buck-Boost chopper to 100 Hz sampling frequency. In contrast, Fig. 6 shows the response of power signals, the duty ratio, and the solar module's voltage at a sampling frequency of 1 kHz.

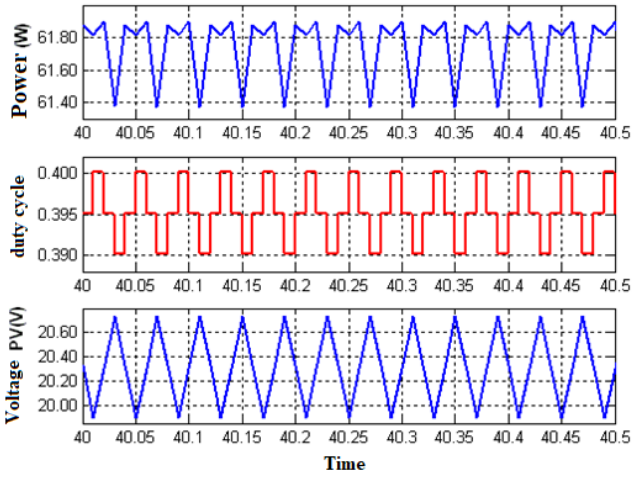


Fig. 5 – Power signals, duty cycle, and voltage PV obtained by the P&O MPPT method applied on a Buck-Boost chopper 100 Hz.

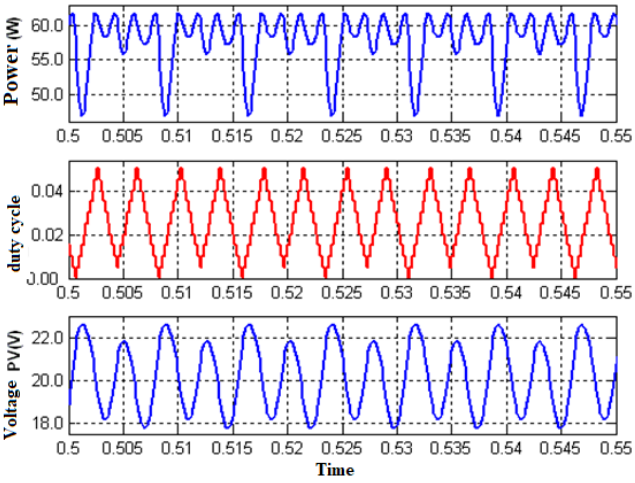


Fig. 6 – Oscillation of the output power, the duty cycle, and the PV voltage obtained by the P&O MPPT control combined with a buck-boost chopper 1 kHz.

So, according to Figs. 5 and 6, the command output and the potential response must behave better. They are oscillatory as those obtained upon application of the buck chopper.

The numerical control at high sample rates harms the PV system. This is seen in the amplitude of the ripple of the power signal, which is slightly increased by one step (Fig. 6) compared with that obtained at 100 Hz (Fig. 5).

### 3.2. THE METHOD OF P&O IMPROVED

The advantage of the method of P&O Improved lies in the fact that the control variable also oscillates about its operational point when the power signal rises. Accordingly,

the controller does not drift in a direction like the conventional method. This reduces the ripple generated at the system level and thus reduces power loss (Fig. 7).

Regardless of the type of chopper used, the P&O MPPT improved method slightly reduces the amplitude of the power ripple at a steady state for sample rates well determined.

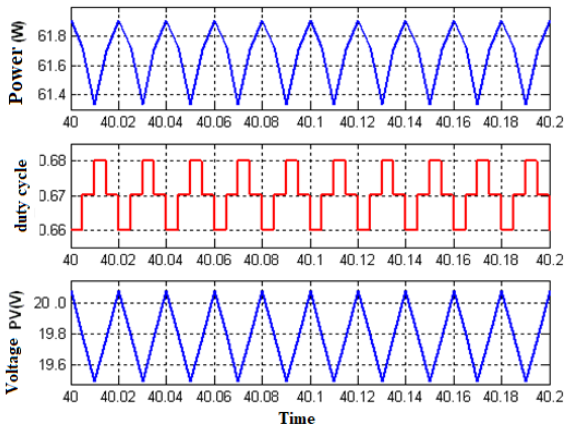


Fig. 7 – The ripple generated at a sampling frequency of 200 Hz, by the P&O improved algorithm combined with a buck chopper.

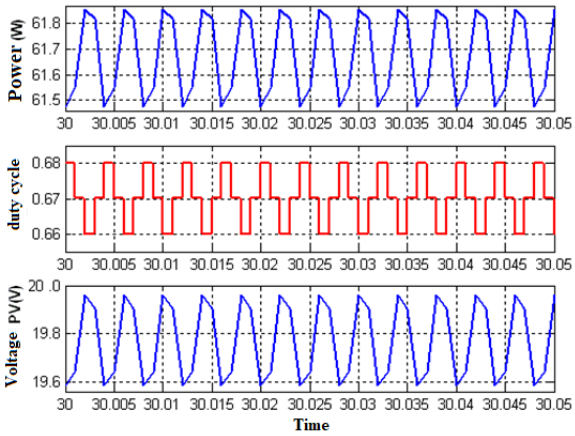


Fig. 8 – Ripple generated at a sampling frequency of 1 kHz, the improved P&O algorithm, combined with a buck chopper.

## 3.3. CONDUCTANCE INCREMENTATION METHOD

Figure 9 shows the power signal and the control variable of a system controlled by the MPPT conductance incrementation algorithm at a sampling frequency of 100 Hz using a buck chopper.

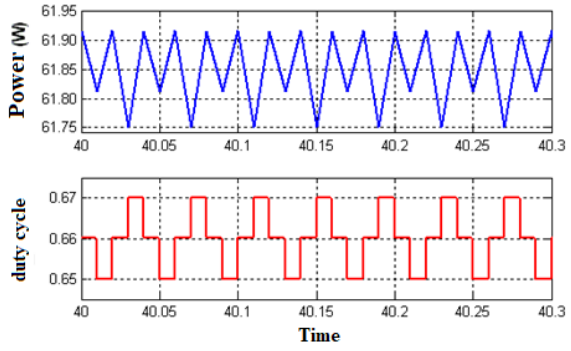


Fig. 9 – Simulation of power and control of the MPPT algorithm IncCond combined with a buck chopper at a sampling frequency of 100 Hz.

The power signal's apparent oscillation shows that the PPM condition $dI/dV = -I/V$ never happens. Satisfaction of this condition by no disturbance when the PPM is achieved would deflect the algorithm.

The approximation of the values ($dI$ and $dV$) and the high resolution of the sampling of the input MPPT controller prevent both satisfying the equation and the conditions $dV = 0$ and $dI = 0$.

Figure 10 shows the response of the conductance incrementing algorithm of the high-frequency oscillation phenomenon. This is an expected phenomenon; since this depends on the system response time varies depending on the type of chopper dc/dc used.

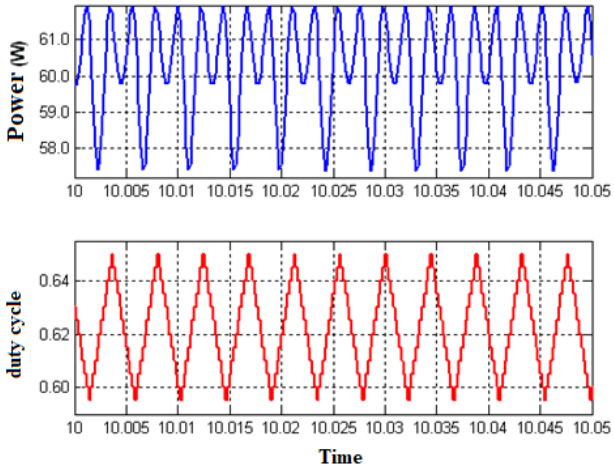


Fig. 10 – Power and control signal simulated by IncCond algorithm combined with a buck chopper at a sampling frequency of 5 kHz.

The information obtained with the simulations discussed so far shows that the increased ripple at higher sample rates MPPT causes a significantly higher power loss.

## 3.4. THE METHOD OF NEURAL NETWORKS

Figure 11 shows the system's response at $T = 25$ °C, $S = 1000$ W/m², and a sampling frequency of 500 Hz. **T**he sample rate does not affect the power loss in the case of a neural controller. This is seen in the power signal and that of the control, where the oscillation phenomenon, which often occurs in conventional controls at high sampling rates (due to the response time of the chopper), has not originated in neuronal control. This amounts to the independence of the neuronal control of the chopper used response time, unlike conventional controls where the controlled assessment often depends on a state variable (voltage, current, and power).

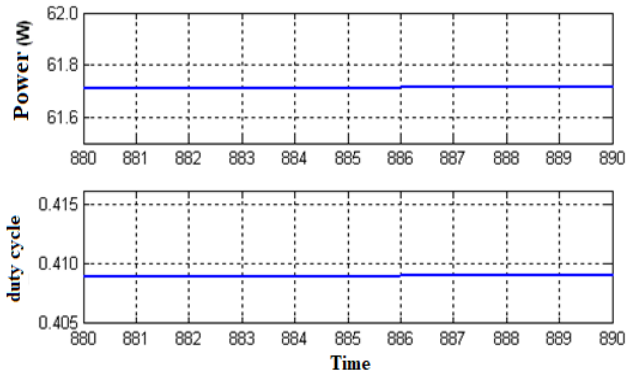


Fig. 11 – Allure of the power and control output of neural Controller combined with a Buck-Boost chopper at 500 Hz.

In practice, the time acquisition signals are tainted by interference or unwanted noise, so the measured signal is always flawed. In our case, we need three sensors, one for temperature and sunshine and the third for the battery

voltage. These measurement signals are injected directly into the neural controller, which requires us to establish a robust controller which always manages to estimate the appropriate command to the presence of noise.

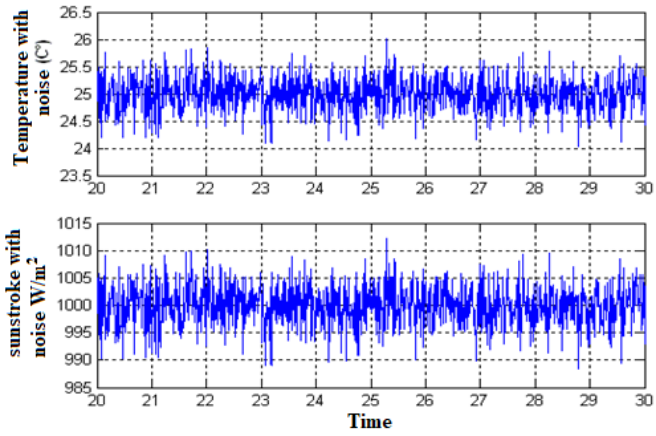


Fig. 12 – Noisy signals of the temperature and sunshine.

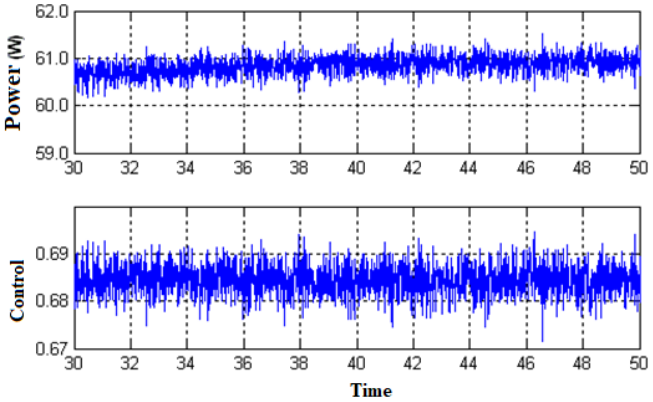


Fig. 13 – Power signals and control system combined with a buck chopper at a sampling frequency of 100 Hz.

We performed a robustness test, injecting the neural controller with two noisy instructions. The first is a signal representing the temperature at 25 °C [38], wherein a Gaussian noise of standard deviation 1 is superimposed on the latter, and the second instruction signal represents the sunlight to 1000 W/m². A Gaussian measurement noise standard deviation of 12 is superimposed on the latter. In contrast, the third input representing the battery voltage is not noisy for practical considerations. Figure 12 shows the input/output signals noisy.

Note from the simulation results shown in Figs. 12 and 13 that the measurement noise superimposed on the signals injected neural controller directly affected the control output, which became noisy. Still, without it, it did not deviate from the actual command he had estimated. Therefore, the neural controller has the robustness to measure noise. The noisy command directly affected the power output with a very low amplitude, which can be estimated as negligible oscillations generated using conventional controls.

## 4. CONCLUSION

The main interest in this work is focused on the power ripple caused by oscillations around the MPP and its dependence on the sampling frequency of various techniques MPPT and the dc-dc converter used, where the sampling frequency limits the controller's speed.

The simulations performed within this article have a purely practical dimension because the only way to evaluate the performance of a digital controller before establishing an actual prototype is to perform a simulation first.

As a result, the simulations provide the best opportunity to evaluate the various MPPT techniques presented in this article and to analyze their behavior under the same operating conditions [36].

This comparative study between different MPPT research techniques [39] allows us to validate the most appropriate for a specific application.

The simulation results clearly show that all the methods can detect the MPP when the temperature and the sunshine vary simultaneously.

Indeed, the performances of the New intelligent control strategy by Neuronal control on the other MPPT commands presented in this article resides, on the one hand, by its speed in estimating the position of the MPP without oscillations, and on the other hand, by obtaining a maximum power without any oscillations and superior to that obtained by the other commands [36] in term of the sampling frequency, particularly when determining photovoltaic system response time, the ripple, and primarily loss of power.

*Received on 29 July 2022*

## REFERENCES

1. S. Issaadi, W. Issaadi, A. Khireddine, *New intelligent control strategy by robust neural network algorithm for real time detection of an optimized maximum power tracking control in photovoltaic systems*, International Journal of Energy, **187**, 15 November 2019, 115881.
2. W. Issaadi, A. Khireddine, S. Issaadi. *Management of a base station of a mobile network using a photovoltaic system*, International Journal of Renewable & Sustainable Energy Reviews (Elsevier), **59**, *C*, pp. 1570–1590 (2016).
3. W. Issaadi, S. Issaadi, A. Khireddine, *Comparative study of the photovoltaic system optimization techniques: Contribution to the improvement and development of a new approach*, International Journal of Renewable & Sustainable Energy Reviews (Elsevier). **82**, *3*, pp. 2112-2127 (February 2018).
4. T. Esram, P.L. Chapman, *Comparison of photovoltaic array maximum power point tracking methods*, IEEE Transactions on Energy Conversion, **22**, *2*, pp. 439–449 (June 2007).
5. V. Salas, E. Olıas, A. Barrado, A. Lazaro, *Review of the maximum power point tracking algorithms for stand-alone photovoltaic systems*", Solar Energy Materials and Solar Cells, **90**, *11*, pp. 1555–1578 (2006).
6. D.P. Hohm, M.E. Ropp, *Comparative study of maximum power point tracking algorithms using an experimental programmable, maximum power point tracking test bed*, IEEE Photovoltaic Specialists Conference, PVSC 2000, pp. 1699-1702 (Sept. 2000).
7. H.D. Maheshappa et al., *An improved maximum power point tracker using a step-up converter with current locked loop*, Renewable Energy, **13**, *22*, pp. 195-201 (1998).
8. S.J. Chiang et al. "Residential Photovoltaic Energy Storage System". IEEE Trans. on I. E., **45**, *3*, pp. 385-394 (June 1998).
9. W. Issaadi *Conventional MPPT and control of a photovoltaic system by neural networks: improvements and perspectives,* Proceedings of the international conference on design and production engineering, 'DPE'2016'. Berlin, Germany (July 25–26, 2016).
10. W. Issaadi et al., *Command of a photovoltaic system by artificial intelligence comparatives studies with conventional controls: Results improvements and perspectives*, IEEE-8th International Conference on Modelling Identification and Control (ICMIC), pp. 583-591 (2016).
11. E. Mujadi, *ANN based peak power tracking for PV supplied dc motors*, Solar Energy, **69**, *4*, pp. 343-354 (2000).
12. R. Akkaya, A.A. Kulaksız, O. Aydogdu, *DSP implementation of a PV system with GAMLP-NN based MPPT controller supplying BLDC motor drive*, Energy Conversion and Management, **48**, *1*, pp. 210–218 (2007).
13. N. Dasgupta, A. Pandey, A.K. Mukerjee, *Voltage-sensing-based photovoltaic MPPT with improved tracking and drift avoidance capabilities*, Solar Energy Materials and Solar Cells, **92**, *12*, pp.

1552–1558 (2008).
14. K-H. Chao, C-J. Li, *An intelligent maximum power point tracking method based on extension theory for PV systems*, Expert Systems with Applications, **37**, *2*, pp. 1050–1055 (2010).
15. A. Oi, *Design and simulation of photovoltaic water pumping system*, Faculty of California Polytechnic State University (2005).
16. W. Issaadi, *Control of a photovoltaic system by Fuzzy Logic, comparative studies with conventional controls: results, improvements, and perspectives,* International Journal of Intelligent Engineering Informatics, **5**, *3*, pp. 206–224 (2017).
17. W. Issaadi, *An improved MPPT converter using current compensation method for PV-Applications*. International Journal of Renewable Energy Research, **6**, *3*. pp. 894-913 (2016).
18. N. Pongratananukul, *Analysis and simulation tools for solar array power systems*, University of Central Florida (2005).
19. T.E. Persen, *FPGA-based design of a maximum-power-point-tracking system for space applications*, University of Florida (2004).
20. R. Kianinezhad, B. Nahid, F. Betin, G.A. Capolino, *A new field oriented control of dual three phase induction machine*s, IEEE International Conference on Industrial Technology, Hammamet, Tunisia (December 2004).
21. Ch. Hua, J. Lin, Ch. Shen, *Implementation of a DSP-controlled PV system with peak power tracking*, IEEE Trans. Ind. Electron., **45**, *1*, pp. 99–107 (1998).
22. S. Qin et al., *Comparative analysis of incremental conductance and perturb-and observation methods to implement MPPT in photovoltaic system*, Wuhan institute of technology, China (2011).
23. Ch. Hua, J. Lin, Ch. Shen, *Implementation of a DSP-controlled PV system with peak power tracking*, IEEE Trans. Ind. Electron., **45**, pp. 99–107 (1998).
24. Z. Salameh, D. Taylor, *Step-up maximum power point tracker for photovoltaic arrays*, Solar Energy, **44**, pp. 57–61 (1990).
25. T.P. Nguyen, *Solar Panel Maximum Power Point Tracker*, Undergraduate Thesis, The University of Queensland Department of Computer Science & Electrical Engineering (19 October 2001).
26. N. Femia, G. Petrone, G. Spagnuolo, M. Vitelli, *Optimization of perturb and observe maximum power point tracking method*, IEEE Transactions on Power Electronics, **20**, *4*, pp. 16-19 (Mar. 2004).
27. K. Noppadol, W. Theerayod, S. Phaophak, *FPGA implementation of MPPT using variable step-size P&O algorithm for PV applications*, Communication and Information Technologies, ISCIT'06, IEEE International Symposium, pp. 212–215 (Sept. 2006).
28. W. Xiao, *A Modified Adaptative Hill Climbing Maximum Power Point Tracking (MPPT) Control Method For Photovoltaic Power Systems*, The University of British Columbia (2003).
29. A. Oi, *Design and Simulation of Photovoltaic Water Pumping System*, Faculty of California Polytechnic State University (2005).
30. E. Koutroulis, K. Kalaitzakis, N.C. Voulgaris, *Development of a microcontroller-based, photovoltaic maximum power point tracking control system*, IEEE Transactions on Power Electronics, **16**, *1*, pp. 46–54 (2001).
31. A.B.G. Bahgat et al., *Maximum Power point tracking controller for PV systems using neural networks*, Renewable Energy, **30**, *8*, pp. 1257–1268 (2005).
32. H. Knopf, *Analysis, Simulation, and Evaluation of Maximum Power Point Tracking (MPPT) Methods for a Solar Powered Vehicle*. Master of Science in Electrical and Computer Engineering, Portland State University (1999).
33. K.H. Hussein, I. Muta, T. Hoshino, M. Osakada, *Maximum photovoltaic power tracking: an algorithm for rapidly changing atmospheric conditions*, IEE Proc. Generation Transmission Distrib., **142**, *1*, pp. 59–64 (1995).
34. K. Ripsaw, T. Saito, I. Takano, Y. Sawada, *Maximum power point tracking control of photovoltaic generation system under non-uniform insolation by means of monitoring cells*, Conf. Record of the Twenty-Eighth IEEE Photovoltaic Specialists Conf., pp. 1707-1710 (2000).
35. G.J. Yu, Y.S. Jung, J.Y. Choi, J.H. Song, G.S. Kim, *A novel two-mode MPPT control algorithm based on comparative study of existing algorithms*, Conf. Record of the Twenty-Ninth IEEE Photovoltaic Specialists Conf., pp. 1531–1534 (2002).
36. J.H. Lee, H. B. Bo, H. Cho, *Advanced incremental conductance MPPT algorithm with a variable step size*, Power Electronics and Motion Control Conference, EPE-PEMC 12th International, pp. 603–607 (Aug. 2006).
37. T.Y. Kim, H.G. Ahn, S.K. Park, Y.K. Le, *A novel maximum power point tracking control for photovoltaic power system under rapidly changing solar radiation*, IEEE International Symposium, **2**, pp. 1011–1014 (Jun. 2001).
38. F. Saftoiu, A.M. Morega, *Cooling system for photovoltaic panels*, Rev. Roum. Sci. Techn. – Électrotechn. Et Énerg., **67**, *3*, pp. 343–348 (2022).
39. M. Burlacu, V. Navrapescu, A-I. Chirila, I-D. Deaconu, *Optimal reactive power management for microgrids based on photovoltaic inverters using sine-cosine algorithm*, Rev. Roum. Sci. Techn. – Électrotechn. Et Énerg., **67**, *2*, pp. 117–122 (2022).